Review of $H_xP_yO_z$–Catalyzed H + OH Recombination in Scramjet Nozzle Expansions; and Possible Phosphoric Acid Enhancement of Scramjet Flameholding, from Extinction of H_3PO_4 + H_2—Air Counterflow Diffusion Flames

Gerald L. Pellett
NASA Langley Research Center, Hampton, VA 23681

Abstract

Recent detailed articles by Twarowski indicate that small quantities of phosphorus oxides and acids in the fuel-rich combustion products of H_2 + phosphine (PH_3) + air should significantly catalyze H, OH and O recombination kinetics during high-speed nozzle expansions -- to reform H_2O, release heat, and approach equilibrium more rapidly and closely than uncatalyzed kinetics. This paper is an initial feasibility study to determine (a) if addition of phosphoric acid vapor (H_3PO_4) to a H_2 fuel jet -- which is much safer than using PH_3 -- will allow combustion in a high-speed scramjet engine test without adverse effects on localized flameholding, and (b) if phosphorus-containing exhaust emissions are environmentally acceptable. A well-characterized axisymmetric straight-tube opposed jet burner (OJB) tool is used to evaluate H_3PO_4 addition effects on the air velocity extinction limit (flame strength) of a H_2 versus air counterflow diffusion flame. Addition of nitric oxide (NO), also believed to promote catalytic H-atom recombination, was evaluated for comparison. Two to five mass percent H_3PO_4 in the H_2 jet increased flame strength 4.2%, whereas airside addition decreased it 1%. Adding 5% NO to the H_2 caused a 2% decrease. Products of H-atom attack on H_3PO_4 produced an intense green chemiluminescence near the stagnation point. The resultant exothermic production of phosphorus oxides and acids, with accelerated H-atom recombination, released sufficient heat near the stagnation point to increase flame strength. In conclusion, the addition of H_3PO_4 vapor (or more reactive P sources) to hydrogen in scramjet engine tests may positively affect flameholding stability in the combustor *and* thrust production during supersonic expansion -- a possible dual benefit with system design / performance implications. Finally, a preliminary assessment of possible environmental effects indicates that scramjet exhaust emissions should consist of phosphoric acid aerosol, with gradual conversion to phosphate aerosol. This is compared to various natural abundances and sources.

Introduction

Background and Scope: Recent experimental / analytic / numerical studies by Twarowski [1-5] strongly suggest that the presence of up to three weight percent phosphorus, as oxides and acids from the well-stirred fuel-rich combustion of H_2 + phosphine (PH_3) + air, should significantly enhance H, OH and O recombination kinetics during high-speed nozzle expansions -- to reform H_2O, release heat, and approach equilibrium more rapidly and closely than uncatalyzed kinetics. Subsequently, Singh et al. [6] adopted Twarowski's detailed recommendations on (mostly unavailable) thermodynamic properties and chemical kinetics, and used an initially-more-divergent hypersonic nozzle geometry to conduct a numerical study of reaction sensitivity, a 1-D finite-rate nozzle thrust evaluation for Mach 18 flows, and a limited uncertainty analysis. The reaction sensitivity study was essentially consistent with Twarowski's findings. The calculated nozzle expansions indicated that chemical thrust equilibrium was approached a little more rapidly compared to Ref. [5]. Two to 8 weight percent phosphorus in fuel-rich combustion products led to predictions of 1 to 4% thrust enhancement with a 30-m long nozzle, after deducting molecular weight penalties [6]. Thus, because modest improvements in scramjet thrust performance appear possible, and these could have relatively large impact on the payload capability of high-speed vehicles, the possibility of achieving useful recombination catalysis needs careful and systematic consideration.

Approved for public release; distribution is unlimited.

It was experimentally straightforward for Twarowski to use gaseous PH_3 mixed with hydrogen in laboratory flow reactor studies [1-3]. And from a functionality standpoint, because PH_3 is pyrophoric, it should enhance even H_2-fueled scramjet combustion, so that flameholding should not be a concern. Unfortunately PH_3 is *very* toxic and its use requires extensive safety precautions, so its practical application as a stored fuel additive becomes extremely difficult and doubtful.

Thus to begin systematic tests of the possibility that phosphorus oxides and acids may improve scramjet thrust performance, while temporarily bypassing the development of relatively safe and efficient phosphorus sources, we chose phosphoric acid vapor as a conveniently safe starting material. However, before attempting to measure catalytic effects on atom-molecule recombination in a nozzle, we need to determine how it might affect high-speed H_2–air combustion / flameholding. Thus while phosphoric acid addition to a scramjet fuel appears much safer for testing thrust enhancement in high speed nozzle expansions, possible adverse effects on scramjet-like flameholding processes need to be examined. In this paper, a previously well characterized 2.7 mm opposed jet burner system was used to measure the flame strength of H_2–air counterflow diffusion flames (via air jet velocity at extinction), with- and without-addition of phosphoric acid vapor to the fuel (and air) sides. Similar experiments were conducted using nitric oxide (NO) addition to the fuel, because NO is also considered a H-atom recombination catalyst. As shown later, a slightly-positive effect on flame strength was found with phosphoric acid vapor, compared to the author's previous experience with various fuel (and air) additives. Finally, the paper concludes with a preliminary assessment of possible environmental effects of phosphorus-containing exhaust emissions.

Review of Catalyzed Recombination Kinetic Studies: Twarowski's five articles represent a detailed and very careful assessment of the influence of phosphorus (oxides and acids) chemistry on the rate of H, OH, and O recombination processes, without the benefit of accurate thermodynamic information or any chemical kinetic data. In the first two studies [1,2] a well-stirred tubular flow reactor was employed to combust H_2, O_2/Ar and phosphine (PH_3) additive. A steady metered supply of reactants produced a steady flow of combustion products through a 38-mm diameter tubular reactor and into a test section consisting of a two-way windowed cube; steadiness was enhanced by exhausting products through a sonic nozzle. The flow was intersected orthogonally by an excimer laser H_2O photolysis beam (193-nm), and either an OH (308-nm) or H_2O (192-nm) probe beam. Combustion flows at 1970 K and 530-590 torr were assumed equilibrated just prior to periodic laser photolyses (10/s) of H_2O.

The first study [1] described: The flow reactor; repetitive measurements of the decay of excess OH absorption over 1 ms, after each 12 ns excimer laser pulse, using a frequency-doubled ring-dye laser OH probe near 306.5-nm; development of a temperature probe based on OH absorption; estimation of the thermochemical properties of 17 phosphorus species (using *ab initio* quantum calculations in many cases); calculation of equilibrium densities under the test conditions; construction of a reaction set that was subsequently reduced to 7 H_xO_y species and 6 $H_xO_yP_z$ species, and 33 reactions; estimation of rate constants, using standard methods for metathesis reactions and simplified Rice-Ramsperger-Kassel-Marcus (RRKM) calculations for the recombination reactions; a sensitivity analysis of the OH decay signal to assumed 10% errors in each of the 20 phosphorus rate constants; a systematic analysis of the final reduced reaction set, including discussion of the considerable uncertainties in heats of formation of key phosphorus species and resultant rate coefficients; and implications of the results for using phosphorus additives in fuels for hypersonic propulsion. Surprisingly, the addition of only 0.1 mole percent PH_3 doubled the OH recombination rate during the first 100-μs of decay. Reaction scheme details are discussed later.

Twarowski's second study [2] described: Photometric determination of the rate of H_2O formation, using the same stirred flow reactor, but with the dye laser OH probe replaced by a H_2O absorption probe consisting of a deuterium lamp and an interference filter at 192-nm; and a demonstration that the 33-reaction model used to describe OH decay in [1] also characterized the growth of

the H_2O signal. Unfortunately, the absorbance of H_2O increased significantly with temperature in the 192 nm region; and the H_2O absorbance change due to heating, from excess photon energy plus H + OH recombination, was *ten* times larger than the absorbance change due to increased H_2O concentration. This 10:1 effect on H_2O absorption coefficient increased both data scatter and uncertainty in the measurement of H_2O, and may have affected the noticeable misfit of time-dependent OH decay and H_2O growth data. As noted by the author, the reaction model put forward "... for the reaction chemistry of high-temperature phosphorus oxide and acid species may be in need of correction."

A third experimental study [3] examined the temperature dependence of H + OH recombination in post-combustion gases, with and without phosphorus oxides, over respective temperature and pressure ranges of 1500-2500 K and 300-700 torr. This study produced a three-body rate coefficient for $H + OH + M \text{ ---> } H_2O + M$, when M is H_2O, that was ten times *larger than expected* at 1500 K, and about ten times *smaller* at 2500 K, with a crossover at 2100 K. The reference rate coefficient used was recommended first by Baulch et al. [7] and later by Warnatz [8]. As pointed out by Twarowski, the actual reference data cannot be interpreted unambiguously; and independent data reported by Bulewicz and Sugden [9] and by Padley and Sugden [10] show a temperature dependence closer to the Ref. [3] results than rate parameters from the Baulch review. If correct, this means that most, if not all, previously reported finite-rate supersonic nozzle flow calculations have *over predicted* H_2O formation in that critical highest-temperature stage of nozzle expansion, where heat release due to recombination has the greatest effect on specific impulse.

The fourth paper [4] details the systematic construction and evaluation of 162 phosphorus reactions, and tests them over a wide range of applicable conditions. Reactions that are even marginally important (defined later) are used to define a reduced reaction set [4]. This paper is far more comprehensive than the Ref. 1 development, which briefly described how a full reaction set was obtained and reduced, the results of a standard sensitivity analysis, and an analysis of OH decay data obtained near 2000 K. Reference 4 starts with the complete listing of 162 possible phosphorus reactions among 17 phosphorus-containing species. It describes the calculation of equilibrium densities (based on very limited thermodynamic data, detailed in [1]), and the calculation methodology used to determine all the rate coefficients. Twarowski used a unique free energy approach to characterize the fractional extent of reaction. He perturbed equilibrium densities by instantaneously decreasing temperature, and also by simulating H_2O photolysis, and then allowed the entire model system to react in each case, minus one reaction at a time. This one-reaction-at-a-time perturbation process identified the relative importance of rate coefficients *as estimated*; and thus it assumed that rate coefficients were not in error by orders of magnitude. The perturbation process was conducted under 36 sets of reaction conditions of possible importance over the entire test region, namely temperatures of 1500-3000 K, densities of $5x10^{-7}$ to $5x10^{-5}$ (equivalent to 1/80 to 5/4 standard atm), and fuel-air equivalence ratios of 0.8, 1.0 and 1.2. Thirty nine of the 162 phosphorus reactions had maximum fractional reaction extents greater than 0.0001 somewhere within the test region, and thus were selected as possibly important. With two minor exceptions, these are identical to the previous reduced set [1]. The maximum extents of reaction for each of the selected reactions are tabulated for both thermal and photolysis perturbations, for each of the 36 conditions. Inspection of the respective tables gives a quick visualization of the relative importance of each reaction under any subset of conditions.

Three sequences of reactions are identified in [1] and [4] that appear to play a key role in the relaxation kinetics of post-combustion gases. The most important sequence, which contributes substantially to the equilibrium relaxation rate over a wide range of reaction conditions, is:

$H + PO_2 + M \text{ ---> } HOPO + M$	(15), Ref. [1] notation
$H + HOPO \text{ ---> } H_2 + PO_2$	(30)
$OH + H_2 \text{ ---> } H_2O + H$	(7)

This sequence gives the overall result, 2H ---> H_2. As pointed out in [4], the large catalytic effect may be due to the large mole fraction of PO_2 in the initial equilibrium mixture; and the activated complex $HOPO^*$ has more degrees of freedom than does HOH^*. The two other reaction sequences provide progressively less favorable paths for H + OH recombination:

$$OH + PO_2 + M \text{ ---> } HOPO_2 + M \quad (21)$$
$$H + HOPO_2 \text{ ---> } H_2O + PO_2 \quad (25)$$

and

$$OH + PO + M \text{ ---> } HOPO + M \quad (20)$$
$$H + HOPO \text{ ---> } H_2O + PO \quad (24)$$

The fifth paper [5] assessed potential reduction of recombination losses during hypersonic expansion of various 2900 K, 1-atm, flows through an 8.6-degree nozzle. Estimated thermodynamic and kinetic parameters for a key subset of 11 phosphorus-containing (and 13 H_xO_y) reactions were used to calculate heat release and departures from equilibrium, and relative specific impulse as a function of phosphorus content (0 to 6 wt. %), initial velocity (3000, 5000, 7000 m/s), and equivalence ratio (0.6 to 6), for static temperatures dropping from 2900 to 1500 K. For fuel-rich combustion, the addition of 2 to 3 weight percent phosphorus substantially increased the calculated heat release per unit mass of fuel. This produced a calculated impulse gain of 3 to 10 s for respective initial reactant temperatures of 1500 to 1000 K.

In Ref. [6] Singh et al. used Twarowski's detailed Ref. [1] recommendations, on thermodynamic properties and chemical kinetics, to conduct a three-part numerical study of reaction sensitivity, and to evaluate Mach 18 expansion characteristics. First, the percent change in characteristic reaction time for each reaction was calculated for 10% perturbations of all rate coefficients, using a chemical Jacobian technique and a representative temperature and pressure. Reaction 30 was found somewhat more important than reaction 15, whereas Ref. [5] found the reverse true over a wide range of conditions. Second, the ratio of longest characteristic reaction times without- and with-added-phosphorus, $t_{max,without\text{-}P} / t_{max,with\text{-}P}$, was calculated as a function of temperature and phosphorus percentage, for fuel-rich and fuel-lean conditions at fixed pressure. These results reinforced Twarowski's finding that the ability of phosphorus to enhance recombination decreases dramatically, and becomes minimal, at temperatures approaching 3000 K. Note that ratios of characteristic reaction times were evaluated under various isothermal conditions, and were decoupled from decreasing pressure during expansion. Third, the same ratio of longest characteristic reaction times was calculated for a *ten-fold* increase in rate of the most sensitive reaction, number 30, H + HOPO ---> H_2 + PO_2. This 1000% increase in rate caused a 25% increase in $t_{max,without\text{-}P} / t_{max,with\text{-}P}$, which implies a 25% improvement in the efficiency of catalysis.

Finally, Singh et al. [6] adopted a representative Mach 18 hypersonic vehicle nozzle, having an initial expansion of 24-degrees for 5.6-m, and an 8.8-degree expansion for the remaining 22.4-m, compared to 8.6-degrees throughout in Ref. [5]. Singh et al. used a quasi 1-D Euler code to evaluate flows for Mach 18 flight, based on nozzle throat conditions of 5364 m/s at a static temperature of 3072 K and pressure of 1 atm. Chemical thrust equilibrium was approached somewhat more rapidly compared to Ref. [5], which was expected due to the greater expansion angle. Two to 8 weight percent phosphorus in the fuel-rich combustion products (1.85 equivalence ratio) led to prediction of 1 to 4% thrust enhancement for a 30-m long nozzle, after deducting molecular weight penalties [6]. For shorter nozzles, maximum thrust enhancement varied with (fuel rich) equivalence ratio at 5% phosphorus content.

Review of H_2–Air Counterflow Diffusion Flame Applications: Strained laminar H_2–air counterflow diffusion flames (CFDFs) have been studied extensively by the author, using various matched pairs of axisymmetric convergent-nozzle (2.7 to 7.2 mm diameter) and straight-tube (1.8 to 10 mm) opposed jet burners (OJBs), and nonintrusive combustion diagnostic techniques [11-19]. Recent comprehensive analyses of velocity- and temperature-field and extinction limit data characterized

major features of the H_2/N_2–*clean* air system from 14 to 100% H_2 [19]. A one-dimensional (1-D) model [15,16] was applied to pre-extinction flame structure [17-19], and also compared with extinction limit data [13,14,19]. Effects of the two different input flow boundary conditions were examined [13,14,17-19]; i.e., the idealized "plug flow" (uniform) axial velocity profile from nozzles, and the fully-developed parabolic profile from tubes (discussed later).

Typically disk-shaped CFDFs are stabilized in a ceramic-fiber combustion box, purged by argon (or helium) bath gas at the bottom and vented through a porous plate at the top (see Fig. 1). Flames are always centered far enough from the jets so they are unanchored or "free-floating" when flows are perturbed slightly. Extinction data are obtained by slowly increasing fuel and air mass flows until the disk flame suddenly ruptures, and forms a ring-shaped flame centered on the stagnation point.

The primary test parameter for a strained CFDF is the exit-area-average air jet velocity, U_{air}, standardized at 0 °C and 1 atm. The U_{air} at extinction is defined as flame strength (FS) [17-19]. From a practical viewpoint, FS in the hydrogen–air system represents the maximum input velocity at which a specific counterflow stagnation flame can process air before the flame fails catastrophically -- due to increasing heat loss, falling temperature, and decreasing reactivity and heat release in the flame. The FS limit for either nozzle- or tube-OJBs (e.g. 2.7 mm) is essentially unaffected by relatively large changes in jet gap, e.g. from one to three exit diameters [13,14,19]. For all reported FS data the disk flame appears essentially 1-D in the central region, just inside the projected exit diameter; although variable curvature typically exists beyond that region, depending on input flows and fuel concentrations, and OJB size and type.

Applied stress rate (ASR) near the outer airside flame edge is approximated globally by a diameter-normalized average air jet velocity; thus ASR applies most strictly along the centerline for large nozzles, and ASR $\approx U_{air}/D_n \approx a_{air}$ [17-19]. For tubes, where flows are 2-D, ASR is directly proportional to U_{air}/D_t, but is effectively larger by an empirical factor of 3 when compared to corresponding axial input strain rates, and in-flame radial strain rates at extinction (in [19], and discussed below).

Various diagnostic techniques were used to quantify the axial, radial and global properties of strained H_2–air diffusion flames. Velocity- and temperature-field results were derived from early Laser Doppler Velocimetry (LDV) and Coherent Antistokes Raman Scattering (CARS) data on tubes [11], and from recent LDV, Particle Imaging Velocimetry (PIV), focusing schlieren and thermocouple data on nozzles and tubes [17-19]. The LDV data demonstrated that, along the axial centerline, maximum input strain rate near the airside edge, $(-du/dx)_e$, was directly proportional to global axial strain rate approximated by $K_{air} = 2U_{air}/D_n$ for nozzles, and $6U_{air}/D_t$ for tubes [19]. This strain rate relationship was particularly notable because the factor of 3 difference was consistent with empirically-correlated extinction limits from various nozzles and tubes, based on K_{air} data [13,14,18,19].

The uniqueness of the H_2–air system requires special experimental considerations, which are particularly important for the present measurements using a 2.7 mm tube-OJB. First, due to the very low flammability limit of H_2 in air, and rapid diffusion of H_2 and H atom, the flame zone outer edge stabilizes on the airside, 8 to 0.6 mm upstream of the stagnation point for 100% H_2, depending on maximum axial input strain rate (100 to 12000 1/s) [16,19]. Thus diffusive combustion proceeds in a strained laminar boundary layer structure, through which air and combustion products flow (see Fig. 1b), *and* the flame experiences a radial strain field that differs somewhat from radial strain at the stagnation point. Presently the exact degree of strain rate offset is not known. Second, very high strain rates are required to achieve extinction of 100% H_2–air -- which is 30 times stronger than CH_4–air [19]. Because axial input strain rate varies as jet velocity divided by diameter, U/D, and Reynolds number (Re) varies as $U D$, achievement of high strain rates *and* laminar flow -- to allow for exact numerical modeling -- requires unusually small nozzles or tubes compared to "conventional" experimental designs. Third, small jet diameters necessitate relatively wide jet gaps ($L \geq 2 D$), to

assure that finite thickness flames are always centered far enough from the jets to be unanchored by heat and/or radical loss mechanisms -- which can seriously degrade the validity of results.

One-dimensional theory has been developed and applied by several researchers to determine the structure and extinction characteristics of various CFDFs [16,20-30]. Unfortunately, the applicability of numerical models for practical input-flow conditions has been limited, and this has impacted OJB selection / use. The two existing 1-D models for axisymmetric opposed jets represent laminar boundary layer approximations, that stem from two different Navier-Stokes stream function solutions [21,23,31] and are most correct at relatively high *Re* near the stagnation point. They apply to either a Hiemenz potential flow input boundary condition (i.e. diverging flow from a distant point source), used first in Ref. 21; or a plug flow input from closely-spaced large-diameter jets, developed first in Ref. 23. For potential flow inputs the applied stress rate, ASR = a_{air}, equals one-half the maximum input axial strain rate near the outer airside edge, $(-du/2dx)_e$, and also radial strain rate near the stagnation point, $(dv/dr)_{sp}$. Potential flow inputs have been used to evaluate the characteristics of methane–air [20,21,23,31] and H_2–air [15,16,21,22,24-26] CFDFs up to extinction. However, non-explicit eigenvalue solutions for plug flow became available somewhat later for methane–air [23]; and only recently for highly-diluted H_2–air [27-29].

Unfortunately the only known 1-D plug flow solutions for large closely-spaced nozzles do not apply to 100% H_2–air extinction data from small nozzle-OJBs, which have gaps much greater than one diameter to prevent flame anchoring [28, and unpublished analyses by G. Balakrishnan]. The missing link is an independent analytic / empirical expression for axial strain rate that applies to small laminar jets with relatively large gap. Such an expression must be based on exit velocity, fluid properties, nozzle diameter, and input H_2 concentration, all of which affect heat release and axial momentum balance at stagnation. Note that flame anchoring is readily simulated in experiments, but always avoided.

Thus, because suitable 1-D numerical models have not been developed to accommodate *either* plug flow *or* parabolic input profiles for systems using high H_2 concentrations [19], the present OJB extinction measurements cannot be compared *exactly* with any 1-D numerical results. However, the very recent demonstration of a generalized 2-D numerical CFDF model that applies for realistic plug or parabolic input flows [30] should facilitate future studies of the input effects.

The validity of using OJB extinction data to assess effects of strain and fuel / air composition on flameholding processes, in a fueled recirculation zone adjacent to much higher speed flow, can be considered from two distinct viewpoints. First the literature and recent results by the author indicate that strain-induced extinction of a 100% H_2–air CFDF is rate-controlled by chemical kinetics in the airside flame, even though hydrogen is transported to the airside by diffusion. The same mechanism applies to N_2-diluted H_2 fuels, down to a certain H_2 concentration range (~ 80%). Below this, extinction limits are also sensitive to decreased H_2 and H atom diffusion caused by inert diluent; and finally by fuel deficiency for H_2 < 29%. Note that recently computed detailed composition and velocity structures clearly illustrate the importance of H_2 diffusion flames on the airside of supersonic laminar-shear-layer flows [32,33]. Second, a primary advantage of (plug flow) axisymmetric CFDFs is that a relatively uniform radial strain rate should exist along any planar isothermal surface located in the impingement flame region [31]. Thus a nozzle OJB, or the central region of a tube-OJB, provides one of the more useful tools available for measuring a macroscopically-uniform strain rate at extinction.

Finally, the author's recent analyses of the H_2/N_2–clean air system [14,19] provide a major baseline for this study, which uses a 2.7 mm nickel tube-OJB, and fuel inputs up to 100% H_2, to measure the effects of phosphoric acid addition on flame strength. The 2.7 mm OJB is preferred for several reasons. Besides being easily fabricated and resistant to mechanical and thermal stress, it is readily adapted to accommodate preheated H_3PO_4 vapor. More importantly it works very well for 100% H_2, in that blowoff occurs cleanly and without obvious defect in the central stagnation region,

resultant mass flow data are highly reproducible, and extinction limits are very insensitive to wide variations in tube separation [13,19]. In agreement with Potter's early observation [34], these robust characteristics are favorably influenced by the parabolic input profile. That is, peak axial velocity creates a stable well-defined impingement flow with maximum strain rate near the center; and very low axial velocity at the jet edge minimizes entrainment of the surrounding bath gas. Note that use of $\geq$ 80% H_2 inputs has always led to asymptotic U_{air} limits at extinction (based on mass flows) which were *insensitive* to (a) increases of linear fuel and air jet input velocities caused by heating, and corresponding decreases in density, (b) jet gap, and (c) the presence of widely different inert bath gases (i.e. Ar, He), which can affect entrainment and diffusion processes near the jet boundary [18,19]. Because the stabilized diffusion flame is located farthest on the airside when 100% H_2 is used, air is convected *through* all phases of the flame zone. Thus the 100% H_2–air CFDF is particularly sensitive to the effects of air additives on thermodynamics and chemical kinetics of flame initiation / propagation [14]. On the other hand, gaseous fuel additives are carried only by diffusion processes beyond the stagnation point, and the rates of H_2, H, and additive specie transport to different regions of the flame depend critically on molecular weight, reactivity and concentration.

Despite the above complexities of transport and reaction, and the present unavailability of exact numerical results for a small tube-OJB, using 100% H_2–air inputs with parabolic input velocity profiles, the experimental approach described below yields idealized measurements that provide direct insight on the proposed efficacy of an H_3PO_4 additive.

Experimental

A schematic diagram of the OJB system, Fig. 1a, illustrates the use of 2.7 mm i.d. nickel tubes more than 50 diameters long. Fig. 1b defines resultant axial and radial combustion flowfields. The ceramic fiber box had two Pyrex windows and a porous sintered metal plate over the top. Argon entering through diffuser jets at the bottom minimized extraneous combustion outside the central impingement region, and thus minimized adverse buoyancy and visibility effects. Air, and fuel component flows of H_2 and N_2 were hand-controlled with micrometer valves, and measured by mass flowmeters previously calibrated at 0 ^oC and 1 atm. The 2.7 mm tubes were spaced 7 mm apart, to ensure a free-floating finite-thickness flame, and mounted horizontally to minimize insulation and flow perturbation, and to allow easy flame restoration after extinction. Flow rates were always high enough that buoyancy effects on the flame were negligible.

To add phosphoric acid vapor to the air or fuel stream, the selected flow was routed through a stainless steel preheat coil into a one-stage stainless steel glass-bead-packed bubbler system, containing about 50-ml of concentrated (85 mass %) meta phosphoric acid. The bubbler system was immersed in a temperature-controlled fluidized bed of hot (80 to 95 °C) sand. Both fuel and air mixtures flowed through coils immersed in the heated fluidized sand, and then through similar electrically-heated coils typically at 100 °C, before entering the OJB. In this manner, phosphoric acid could be introduced successively into respective fuel and air mixtures, with both 'clean air' and 'clean fuel' controls, and condensation was prevented before combustion. Unfortunately the H_3PO_4 content of respective fuel and air streams was not measured accurately. Instead it was estimated using vapor pressure as an initial guideline, and then by quantity of acid consumed per cumulative gas flow during a run sequence. Although phosphoric acid vapor concentrations probably varied between 2 and 5 mass percent over each series of runs, there was no perceptible change in flame strength with time, or when the H_3PO_4 bubbler was cleaned and recharged.

To obtain each extinction data point after the flow system was connected and stabilized, and the counterflow flame was ignited and centered, the flow of H_2 was gradually increased -- or fixed at a target rate when N_2 fuel diluent was increased instead. Simultaneously the air flow was gradually increased, so the flame was always centered and free-floating. After blowoff, or sudden rupture of the

airside disk flame from the center outward, a residual ring flame formed and quickly relocated about the stagnation point. Mass flows of each component were recorded, and the disk flame was slowly restored (and recorded) to prepare for the next extinction measurement.

The reported area-average jet velocities, U_{air} and U_{fuel}, were calculated from component mass flow rates standardized at 0 °C and 1 atm, and tube exit diameter, and are expressed at those conditions. Corresponding Re_{air} were generally less than 1500, but were not so low that CFDFs became excessively thick or non-axisymmetric.

Errors in extinction limits stemmed from various sources. Because actual jet velocities at extinction are predicted [24-26] to vary linearly with input temperature up to about 600 K, and are found to vary approximately linearly (unpublished data), mass flow measurements largely negated the effects of variations in actual jet temperature, pressure and velocity (via the ideal gas law). Thus data scatter was significantly reduced. Calculated jet velocities were sensitive to (measured) jet diameter squared, and applied stress rates (ASRs) were sensitive to diameter cubed. Because visible flame thicknesses were at least 1-mm, and flame offsets from the stagnation point were nearly 2-mm (unpublished measurements), some degree of non-ideality and uncertainty is associated with the 2.7 mm tube-OJB, as discussed earlier. Importantly for the present study, phosphoric acid data were obtained over less than a month to minimize uncertainties associated with mass flowmeter drift. Residual differences between 1994 phosphoric acid data, the 1992 nitric oxide data (discussed later), and 1988 clean air sets are due typically to minor differences in OJB construction, argon purge flows / geometry, and mass flowmeter usage and recalibrations, over time.

In summary, a previously characterized 2.7 mm tube-OJB was used to assess the effects of phosphoric acid vapor addition to the fuel jet on strain-induced extinction limits of H_2–air CFDFs. Phosphoric acid vapor was added respectively to the fuel and air sides, and both clean-fuel and clean-air (bypass) baselines were obtained. The same OJB tool was used to assess the effect of nitric oxide addition to the fuel jet, to provide a direct comparison with a second substance known to have catalytic H-atom recombination activity.

Results and Discussion

Figure 2 shows a typical plot of U_{air} extinction (and flame restoration) data versus $X(H_2)$ and U_{fuel}, obtained previously for clean air [13] using a 2.7 mm tube-OJB. Some unique features are evident, as discussed in [13,14,19]. First, blowoff and restore are separated by a large hysteresis. Second, the 2.7 mm U_{air} blowoff data increase linearly at low $X(H_2)$, but become non-linear beyond 50% H_2. A well defined horizontal U_{air} asymptote is achieved for 80 to 100% H_2, where a near doubling of U_{fuel} reflects the input jet momentum balance needed to center a flame. The extinction limit for $\geq$ 80% H_2 reflects a regime of kinetically-limited H_2 combustion, unaltered by differing H_2 diffusion from the fuel side, but proportional to the O_2 content of air [14]. Note this asymptote (527 cm/s) was obtained much earlier (1988) and is slightly larger than the present value (494 cm/s in 1994, shown below), obtained using different mass flowmeters / calibrations and a different combustion box, but the same OJB tubes. Since 1988 average U_{air} asymptotes have drifted downward to just below 500 cm/s; a grand average of 15 independent asymptotes from 1986 to 1996 using the same OJB tubes, is 505 $\pm$ 17 cm/s.

Fig. 3 shows the full set of flame strength data obtained with- and without-addition of 2 to 5 mass percent H_3PO_4 vapor to the fuel premix or air jets. Although the data cover a wide range of H_2 concentrations in the H_2 + N_2 fuel premix, major conclusions are derived from the asymptotic region, 77% to 100% H_2. Inspection of this region indicates that addition of H_3PO_4 to the fuel jet produced a higher flame strength limit. This delineation becomes much clearer in Fig. 4, which magnifies the asymptotic region. Respective sets of baseline results for 'clean air,' 'clean fuel,' and results for air + H_3PO_4, are clearly lower than replicated results for fuel containing H_3PO_4. Finally, data from the

respective sets were averaged, and results are summarized in Fig. 5. Error bars correspond to standard errors of the data mean over the asymptotic region. Clearly, the small additions of phosphoric acid vapor to the H_2 jet increased flame strength by about 4.2%.

For both lightly-strained flames and those near extinction, the phosphoric-acid-seeded H_2 stream plainly exhibits the effect of H-atom attack, which produces a mixture of H_xPO_y products and yields an intense green chemiluminescence near the stagnation point. This is because H-atom is very reactive, and is essentially the only H_xO_y radical present on the fuel side of stagnation. For example, numerical simulations of the unseeded pre-extinction concentration field [15,21,22,24] show clearly [15] that H-atom concentration begins to rise about 0.15-mm on the fuel side of stagnation, attains about 1/4 maximum concentration at stagnation (0-mm), and continues rising to a maximum near 0.30-mm on the airside; *but* both OH and O atom only begin to appear about 0.15-mm on the airside, and maximize upstream at about 0.40-mm. Peak temperatures of about 1400 K are attained near 0.35-mm on the airside. Thus it appears likely that H_3PO_4 first reacts exothermically with H-atoms. An initial reaction / degradation sequence dependent on H atoms may involve:

$H + (HO)_3PO \rightarrow (HO)_2PO_2 + H_2$
$H + (HO)_2PO_2 \rightarrow HOPO_3 + H_2$
$H + HOPO_3 \rightarrow H_2O + PO_3$
$H + PO_3 \rightarrow O + HOPO$
$H + PO_3 \rightarrow OH + PO_2$
$H + PO_3 + M \rightarrow HOPO_2 + M$
$H + HOPO_2 \rightarrow H_2O + PO_2$

Subsequently the H_xPO_y intermediates are expected to continue reacting exothermically with H atoms, and to promote catalytic H-atom recombination near the stagnation point. Upstream recombination of H, OH and O to form H_2O may also be enhanced, but the effect may be secondary. Thus the resultant processes consume H-atoms, increase heat release near stagnation, and increase flame strength. Based on the velocity field [16-19], this probably occurs over the last 20 to 50 microseconds of burnt gas flow near stagnation.

Finally, an additional series of relative-flame-strength experiments was performed to (a) determine a possible catalytic effect of nitric oxide (NO) in the fuel jet, relative to N_2 diluent (inert under extinction conditions), and (b) assess the relative catalytic effect of NO compared to phosphoric acid. When NO was added to the fuel jet a red chemiluminescence was observed near the stagnation point. Fig. 6 shows measured flame strengths, for which either NO or N_2 were blended with H_2 (without preheating), using the 2.7 mm tube-OJB. These experiments were performed over a one-week period, to minimize relative uncertainty, but with an earlier (2 years) flowmeter / calibration configuration that had a slightly different clean-air baseline. The results indicate that progressive addition of NO to the fuel jet (0 to 15 mole %) decreased flame strength by 0.40% / (mole % NO). Although this decrease is significant, it is not considered large. (For example, in similar experiments using the same OJB [13], the addition of methane to H_2 caused flame strength to decrease 2.2% / (mole % CH_4), which is a much larger H atom scavenging effect because resultant CH_3 radical is relatively unreactive.)

Nevertheless, the negative effect of NO addition in Fig. 6 was somewhat unexpected because the presence of relatively small (< 5%) amounts of NO has been proposed [35,36], and deduced from analysis of scramjet engine tests [37], to have a modest enhancement effect on H and OH recombination kinetics in hypersonic nozzle expansions. Three of the important catalytic reactions are:

$H + NO + M \rightarrow HNO + M$
$H + HNO \rightarrow H_2 + NO$
$OH + HNO \rightarrow H_2O + NO$

The first two reactions of this catalytic cycle are analogous to the two most important phosphorus reactions for recombination in nozzle flows, numbers 15 and 30. To explain the role of NO in the OJB experiments, we first note that an initial exothermic H-atom attack on a large molecule like H_3PO_4 is missing. However, H-atom consumption with formation of HNO initiates on the fuelside, and is followed by further H atom recombination, H_2O formation, and resultant heat release. Obviously, however, the incremental H atom recombination and heat release effect of NO addition is not strong enough to increase flame strength above the clean fuel level, regardless of NO concentration.

A direct comparison of the NO results in Fig. 6 with the phosphoric acid results in Fig. 4 and 5 suggests that phosphoric acid has a significantly stronger effect on the flame strength of a "standard" H_2–air counterflow diffusion flame. Note that because the jet inputs in each case are near ambient temperature, peak flame temperatures for the pure H_2–air CFDFs should be near 1400 K just before extinction [15,21,22,24-26]. Higher peak temperatures are attainable with increased input temperatures, but this was not attempted in the present study.

Based on our present knowledge of flame dynamics and kinetics, it is concluded that phosphorus oxides and acids and H_2 were initially produced by exothermic H-atom attack on phosphoric acid. This resulted in enhancement of H-atom (and possible OH radical) recombination, possible enhanced H_2O formation, and release of additional heat near the final-stage of stagnation-point flow of H_2–air flames. Additionally, the catalytic effect of added phosphoric acid was significantly larger than that for added NO, which produced HNO and caused a similar but reduced acceleration of heat release due to H and OH recombination.

Environmental Impact of Phosphoric Acid Addition to Scramjet Fuels:

A review of phosphorus chemistry suggests that phosphoric acid aerosol will quickly form when the combustion products of a "phosphorus-seeded fuel" airbreathing scramjet engine expand, cool and mix with air. This should occur at virtually any altitude in the troposphere, because (1) substantial water vapor concentrations will exist in the exhaust plume, and (2) virtually all phosphorus oxides and acids have relatively low vapor pressure, and are very reactive with O_2 and $H_2O(g)$. Resultant hydrated solids and liquids are exceptionally hygroscopic, and will combine with atmospheric water vapor to form aqueous H_3PO_4 aerosol. The low vapor pressure of H_3PO_4 and its hygroscopicity at ambient temperature will stabilize aqueous aerosol content in near-equilibrium with local water vapor concentration, which can vary widely with location. For stationary emissions at a ground test facility, corrosion due to phosphoric acid will tend to occur on certain unprotected surfaces, similar to that for sulfuric acid mist in a power plant facility.

Over time, acid aerosol will react with available bases in the atmosphere, such as NH_3 (g) and/or metal oxides or cations such as Ca^{++} or Mg^{++}, to form various soluble and insoluble phosphates in aerosol droplets, or near-solid particles under very dry conditions like $(NH_4)_xH_{3-x}PO_4 \cdot nH_2O$. Due to the similarity of sulfuric acid chemistry with that for phosphoric acid, phosphate aerosol chemistry should follow the well known behavior of sulfate aerosol, whether from volcanic activity or from surface pollution sources.

The ultimate fate of phosphate aerosol in the troposphere should parallel that of sulfate aerosol, in which reaction with basic substances, rainout, washout and dry deposition to the earth's surface will tend to remove the aerosol after an atmospheric halflife of several hours to a few days. Note that phosphorus occurs naturally on the earth's surface, primarily as orthophosphates $[PO_4]^{3-}$. Calcium, iron, aluminum and certain clay minerals readily unite with soluble phosphorus to render it insoluble [38].

For tropospheric emissions from airbreathing vehicles, resultant phosphate aerosol will be widely dispersed, so that eutrophication of various ground receivers will be minimal, compared with other

airborne pollutants. For stationary test facility sources emitting near ground level, effects will be much more local, and could be negligible or quite significant, depending on intensity and duration of emissions, and presence / absence of scrubbers or neutralizing sprays.

To consider the impact of multiple airbreathing vehicle flights, it is useful to assess the natural abundance and source strengths of phosphorus, and compare them with sulfur. In the marine biosphere, the abundance of P and S are comparable (1300 versus 1400 parts per million by mass, ppm), but the abundance of P in seawater is much smaller (0.07 versus 885) because P is a limiting nutrient [38]. The abundance of P in alfalfa grass is 7010 ppm, compared to 1040 ppm for S [38]. Considering possible volcanic and meteoric sources in the upper atmosphere, the gross abundance of P, which exists as $[PO_4]^{3-}$ in igneous rocks, is 1000 ppm ± 300, compared to 1800-1900 ppm in meteoric material, and a gross abundance of 1000-1200 ppm at the earth's surface [38]. Finally, because the abundance of P in the earth's lithosphere is 1180 ppm, compared to 520 ppm for S [38], volcanic emissions of phosphorus compounds may be somewhat larger compared to volcanic sulfur emissions such as H_2S, SO_2, H_2SO_4 and sulfate.

In summary, phosphoric acid aerosol will be the primary emission product resulting from introduction of phosphorus to the H_2 fuel of an airbreathing scramjet engine, and it will gradually convert to soluble / insoluble phosphate aerosol in the atmosphere. Although local pollution and significant corrosion problems may result from ground tests if emissions are large and are not scrubbed or neutralized with alkaline sprays, emissions from infrequent flight in the troposphere should have relatively little additional impact compared to existing natural and anthropogenic pollution sources.

Concluding Statements

1. Twarowski's detailed and very careful assessment of the influence of phosphorus (oxides and acids) chemistry on the rate of H, OH, and O recombination processes appears remarkably good, especially without the benefit of accurate thermodynamic information or any chemical kinetic data. Although the flow reactor data were obtained near 2000 K, the most critical region for recombination is several hundred degrees higher. Also, the UV water vapor measurement had significant uncertainty because absorbance was very sensitive to temperature; use of a less sensitive spectral region would improve H_2O production data, and possibly the chemical kinetic assessment. Additional measurements of PO_2 and/or HOPO under high-temperature equilibrium conditions would provide a critical test of the thermodynamic data. Finally, a relatively safe and efficient source of phosphorus is needed.

2. The addition of 2 to 5 mass percent phosphoric acid vapor to the fuel jet of a H_2–air counterflow diffusion flame enhances the air jet velocity extinction limit (flame strength) by about 4 percent. This appears to be caused by exothermic H-atom attack on phosphoric acid, catalytic H-atom recombination, possible additional H_2O formation, and resultant additional heat release, all near the stagnation point. Similar addition of nitric oxide, which is also believed to catalyze H-atom recombination, decreases flame strength slightly -- apparently because there is no initial exothermic H-atom attack on a large molecule, and the catalytic effect is weaker.

3. Addition of phosphoric acid vapor (or other more active P sources) to hydrogen in scramjet engine tests may positively affect *both* flameholding stability and subsequent thrust production during supersonic expansion -- a possible dual benefit with system design / performance implications.

4. The environmental effects of scramjet exhaust emissions containing a few percent phosphorus were briefly assessed. Resultant phosphoric acid / phosphate aerosol from infrequent tests in the troposphere should have relatively little additional impact compared to existing sources and abundances. Also, infrequent tests in the stratosphere should be acceptable enough to allow future feasibility tests of phosphorus catalysis for scramjet thrust enhancement.

Acknowledgments

The author gratefully acknowledges the careful, consistent support by Lloyd G. Wilson in designing, constructing and operating the OJB systems, and assisting with student mentoring. Two highly-motivated Virginia Governor's School students participated directly in the acquisition and analysis of data. Ms. Angeline G. Lim conducted the nitric oxide studies, and Ms. Theresa J. Debban conducted the phosphoric acid studies. The author is grateful for their substantial efforts.

References

1. Twarowski, Alan, "The Influence of Phosphorus Oxides and Acids on the Rate of H + OH Recombination," *Combustion and Flame*, 94:91-107 (1993).

2. Twarowski, Alan, "Photometric Determination of the Rate of H_2O Formation from H and OH in the Presence of Phosphine Combustion Products," *Combustion and Flame*, 94:341-348 (1993).

3. Twarowski, Alan, "The Temperature Dependence of H + OH Recombination in Phosphorus Oxide Containing Post-Combustion Gases," *Combustion and Flame*, 105:407-413 (1996).

4. Twarowski, Alan, "Reduction of a Phosphorus Oxide and Acid Reaction Set," *Combustion and Flame*, 102:41-54 (1995).

5. Twarowski, Alan, "The Effect of Phosphorus Chemistry on Recombination Losses in a Supersonic Nozzle," *Combustion and Flame*, 102:55-63 (1995).

6. Singh, D. J., Carpenter, M. H., and Drummond, J. P., "Thrust Enhancement in Hypervelocity Nozzles by Chemical Catalysis," *J. Propulsion and Power*, Technical Note (accepted for publication, Nov., 1996).

7. Baulch, D.L., Drysdale, D.D., Horne, D.G., Lloyd, A.C., *Evaluated Kinetic Data for High Temperature Reactions*, Vol. 1, Butterworths, London, 1972.

8. Warnatz, J., in *Combustion Chemistry*, edited by W.C. Gardiner, Jr., Springer-Verlag, New York, 1984, pp. 197-360.

9. Bulewicz, E.M. and Sugden, T.M., Trans. Farad. Soc., 54:1855-1860 (1958).

10. Padley, P.J. and Sugden, T.M., Proc. Royal Soc. London, 248:248-265 (1958).

11. Pellett, G. L., Northam, G. B., Wilson, L. G., Jarrett, O., Jr., Antcliff, R. R., Dancey, C. L., and Wang, J. A., "Opposed Jet Diffusion Flames of Nitrogen-Diluted Hydrogen vs. Air: Axial LDA and CARS Surveys; Fuel/Air Strain Rates at Extinction," AIAA-89-2522, July, 1989.

12. Pellett, G. L., Wilson, L. G., Northam, G. B., Guerra, Rosemary, "Effects of H_2O, CO_2, and N_2 Air Contaminants on Critical Airside Strain Rates for Extinction of Hydrogen–Air Counterflow Diffusion Flames," Presented at 26th JANNAF Combustion Meeting, Pasadena, CA, Oct., 1989. CPIA Pub. 529, Vol. II, Oct. 1989, pp. 23-42.

13. Pellett, G. L., Northam, G. B., Wilson, L. G., "Counterflow Diffusion Flames of Hydrogen, and Hydrogen Plus Methane, Ethylene, Propane, and Silane, vs. Air: Strain Rates at Extinction," AIAA-91-0370, Jan., 1991.

14. Pellett, G. L., Northam, G. B., and Wilson, L. G., "Strain-Induced Extinction of Hydrogen–Air Counterflow Diffusion Flames: Effects of Steam, CO_2, N_2, and O_2 Additives to Air," AIAA-92-0877, Jan., 1992.

15. Isaac, K. M., Ho, Y. H., Zhao, J., Pellett, G. L., and Northam, G. B., "Global Characteristics and Structure of Hydrogen-Air Counter Flow Diffusion Flame: A One-Dimensional Model," AIAA-94-0680, Jan., 1994.

16. Zhao, J., Isaac, K.M., and Pellett, G.L., "Global Characteristics and Structure of Hydrogen-Air Counter flow Diffusion Flames," *J. Propulsion Power*, 12:534-542 (1996).

17. Pellett, G. L., Roberts, W. L., Wilson, L. G., Humphreys, W. M., Jr., Bartram, S. M., Weinstein, L.M., and Isaac, K. M., "Structure of Hydrogen–Air Counterflow Diffusion Flames Obtained by Focusing Schlieren, Shadowgraph, PIV, Thermometry, and Computation," AIAA 94-2300, June 1994.

18. Pellett, G. L., Wilson, L. G., Humphreys, W. M., Jr., Bartram, S. M., Gartrell, L. R., and Isaac, K. M., "Velocity Fields of Axisymmetric Hydrogen–Air Counterflow Diffusion Flames from LDV, PIV, and Numerical Computation," AIAA-95-3112, July 1995.

19. Pellett, G. L., Isaac, K. M., Humphreys, W. M., Jr., Gartrell, L. R., Roberts, W. L., IV, Dancey, C. L. and Northam, G. B., "Velocity and Thermal Structure, and Strain-Induced Extinction of 14 to 100% Hydrogen–Air Counterflow Diffusion Flames, Acceptable for publication with revisions, Jan. 1997.

20. Dixon-Lewis, G., David, T., Gaskell, P. H., Fukutani, S., Jinno, H., Miller, J. A., Kee, R. J., Smooke, M. D., Peters, N., Effelsberg, E., Warnatz, J., and Behrendt, F., "Calculation of the Structure and Extinction Limit of a Methane-Air Counterflow Diffusion Flame in the Forward Stagnation Region of a Porous Cylinder," *Twentieth Symposium (International) on Combustion*, 1984, pp. 1893-1904.

21. Dixon-Lewis, G., David, T., and Gaskell, P. H., "Structure and Properties of Methane-air and Hydrogen-air Counterflow Diffusion Flames," *Archivum Combustionis*, 6, No. 1, 1986, pp. 3-21.

22. Dixon-Lewis, G., and Missaghi, M., "Structure and Extinction Limits of Counterflow Diffusion Flames of Hydrogen-Nitrogen Mixtures in Air," *Twenty-Second Symposium (International) on Combustion*, 1988, pp. 1461-1470.

23. Key, R. J., Miller, J. A., Evans, G. H., and Dixon-Lewis, G., "A Computational Model of the Structure and Extinction of Strained, Opposed Flow, Premixed Methane-Air Flames," *Twenty-Second Symposium (International) on Combustion*, 1988, pp. 1479-1494.

24. Gutheil, E. and Williams, F., "A Numerical and Asymptotic Investigation of Structures of Hydrogen-Air Diffusion Flames at Pressures and Temperatures of High-Speed Combustion," *Twenty-Third Symposium (International) on Combustion*, 1990, pp. 513-521.

25. Gutheil, E., Balakrishnan, G., and Williams, F. A., "Structure and Extinction of Hydrogen-Air Diffusion Flames," in *Reduced Kinetic Mechanisms for Application in Combustion Systems*, edited by N. Peters and B. Rogg, Springer, 1992, p. 177.

26. Darabiha, N., and Candel, S., "The Influence of the Temperature on Extinction and Ignition Limits of Strained Hydrogen-Air Diffusion Flames," *Combustion Science and Technology*, 86, pp. 67-85 (1992).

27. Balakrishnan, G., "Studies of Hydrogen-Air Diffusion Flames and of Compressibility Effects Related to High Speed Propulsion," Ph. D. Dissertation, University of California, San Diego, La Jolla, CA, 1992.

28. Balakrishnan, G., Trees, D., and Williams, F.A., "An Experimental Investigation of Strain-Induced Extinction of Diluted Hydrogen–Air Counterflow Diffusion Flames," *Combustion and Flame*, 98, pp. 123-126 (1994).

29. Papas, P., Glassman, I., and Law, C.K., "Effects of Pressure and Dilution on the Extinction of Counterflow Nonpremixed Hydrogen–Air Flames," *Twenty-Fifth Symposium (International) on Combustion*, 1994, pp. 1333-1339.

30. Zhao, J. and Isaac, K. M., "Influence of Geometry and Heat Release on Counterflow Diffusion Flames: A Navier-Stokes Model," AIAA Paper 95-0133, Jan., 1995.

31. Dixon-Lewis, Graham, "Structure of Laminar Flames," Invited Lecture, *Twenty-Third Symposium (International) on Combustion*, 1990, pp. 305-324.

32. Im, H. G., Chao, B. H., Bechtold, J. K., and Law, C. K., "Analysis of Thermal Ignition in the Supersonic Mixing Layer," *AIAA Journal*, 32:341-349 (1994).

33. Nishioka, M. and Law, C. K., "A Numerical Study of Ignition in the Supersonic Hydrogen/Air Laminar Mixing Layer," AIAA 95-0377, Jan. 1995.

34. Potter, A. E., Heimel, S., and Butler, J. N., "Apparent Flame Strength, A Measure of Maximum Reaction Rate in Diffusion Flames," *Eighth Symposium (International) on Combustion*, The Combustion Institute, Pittsburgh,1962, pp. 1027-1034.

35. Jachimowski, Casimir J., "An Analysis of Combustion Studies in Shock Expansion Tunnels and Reflected Shock Tunnels," NASA TP-3224, 1992.

36. Jachimowski, Casimir J., "Chemical Kinetic Research Related to Combustion in High-Speed Flows," in *Major Research Topics in Combustion*, Hussaini, M. Y., Kumar, A., and Voigt, R. G., editors, Springer-Verlag, New York, 1992, pp. 339-355.

37. Fischer, Karen E., and Rock, Kenneth E., "Calculated Effects of Nitric Oxide Flow Contamination on Scramjet Performance," AIAA 95-2524, July, 1995.

38 . *The Encyclopedia of Geochemistry and Environmental Sciences*, in *Encyclopedia of Earth Sciences Series*, Volume IVA, edited by Rhodes W. Fairbridge, Van Nostrand Reinhold, New York, 1972.

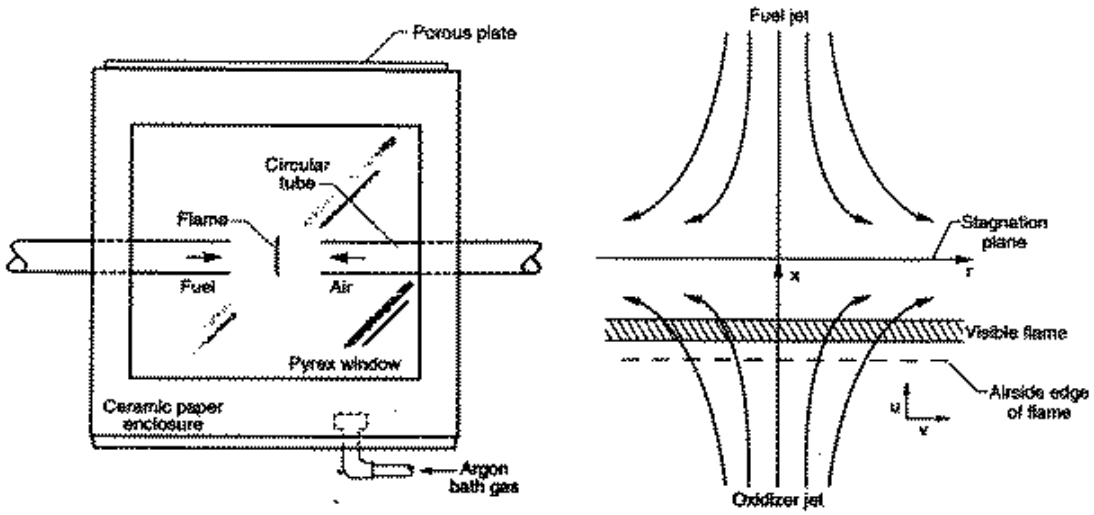

Fig. 1. (a) Tube-OJB oriented horizontally. The interlocked / stapled Fiberfrax® enclosure had a porous metal plate on top, a V-shaped tube holder, and multiple inert gas jets near the bottom. (b) Schematic of axial-radial flowfield of a H_2/N_2-air CFDF.

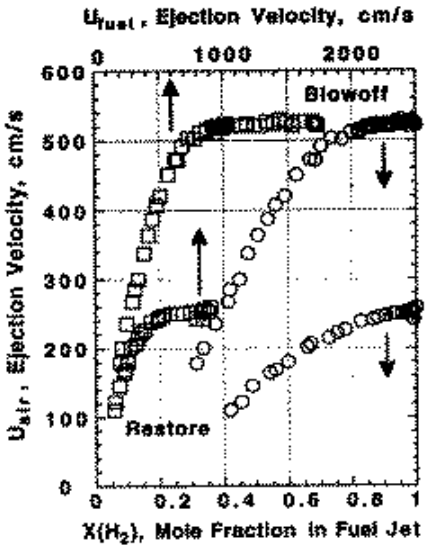

Fig. 2. Cross plot of air and fuel jet velocities for extinction (blowoff) and restoration limits of H_2/N_2-air CFDFs, using 2.7 mm tube-OJB.

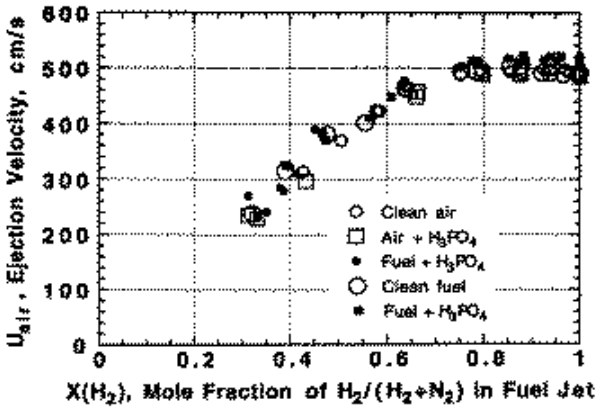

Fig. 3. Phosphoric acid effect on extinction of H_2/N_2-air CFDFs, for fuel + H_3PO_4, air + H_3PO_4, and "clean" fuel / air controls, using 2.7 mm tube-OJB. The H_3PO_4 varied 2 to 5 mass percent.

15

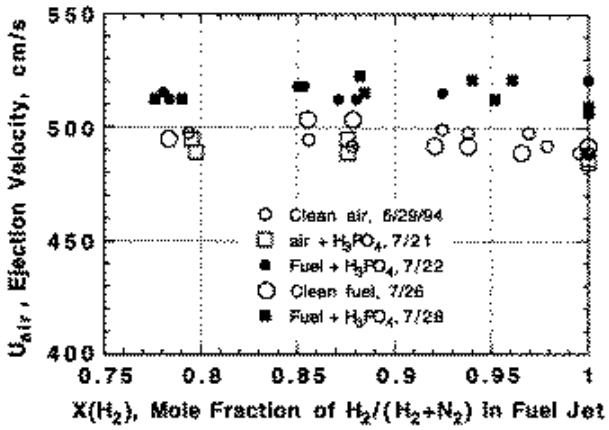

Fig. 4. Magnified view of Fig. 3 asymptotic data, showing effect of 2 to 5 mass percent phosphoric acid vapor on extinction of H_2/N_2–air CFDFs.

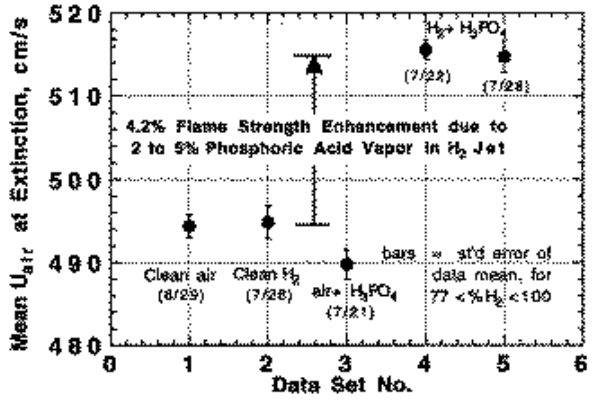

Fig. 5. Averaged asymptotic data from Fig. 4, showing effect of 2 to 5 mass percent phosphoric acid vapor on extinction of H_2/N_2–air CFDFs.

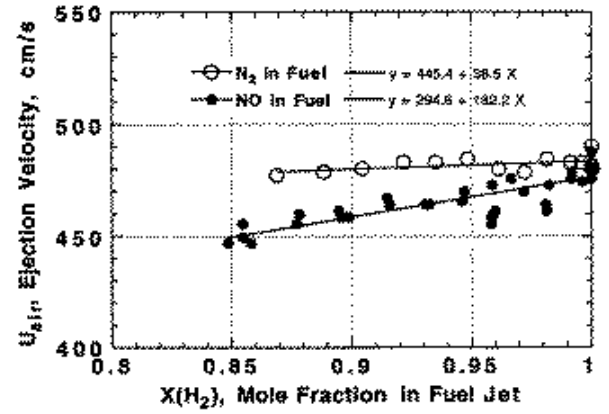

Fig. 6. Effect of nitric oxide added to fuel on extinction of H_2/N_2–air CFDFs, using 2.7 mm tube-OJB.

16